Journal of Materials Chemistry B

Accepted Manuscript

ROYAL SOCIETY OF CHEMISTRY

www.rsc.org/materialsB

Journal of Materials Chemistry B

ARTICLE

Development of Superoxide Dismutase Mimetic Surfaces to Reduce Accumulation of Reactive Oxygen Species for Neural Interfacing Applications

Cite this: DOI: 10.1039/x0xx00000x

Received 22nd January 2014,
Accepted ????

DOI: 10.1039/x0xx00000x

www.rsc.org/

Kelsey A. Potter-Baker[a,b ψ], Jessica K. Nguyen[a,b ψ], Kyle M. Kovach[b], Martin M. Gitomer[a], Tyler W. Srail[a], Wade G. Stewart[a], John L. Skousen[a,b] and Jeffrey R. Capadona[a,b*]

Despite successful initial recording, neuroinflammatory-mediated oxidative stress products can contribute to microelectrode failure by a variety of mechanisms including: inducing microelectrode corrosion, degrading insulating/passivating materials, promoting blood-brain barrier breakdown, and directly damaging surrounding neurons. We have shown that a variety of anti-oxidant treatments can reduce intracortical microelectrode-mediated oxidative stress, and preserve neuronal viability. Unfortunately, short-term soluble delivery of anti-oxidant therapies may be unable to provide sustained therapeutic benefits due to low bio-availability and fast clearance rates. In order to develop a system to provide sustained neuroprotection, we investigated modifying the microelectrode surface with an anti-oxidative coating. For initial proof of concept, we chose the superoxide dismutase (SOD) mimetic Mn(III)tetrakis(4-benzoic acid)porphyrin (MnTBAP). Our system utilizes a composite coating of adsorbed and immobilized MnTBAP designed to provide an initial release followed by continued presentation of an immobilized layer of the antioxidant. Surface modification was confirmed by XPS and QCMB-D analysis. Antioxidant activity of composite surfaces was determined using a Riboflavin/NitroBlue Tetrazolium (RF/NBT) assay. Our results indicate that the hybrid modified surfaces provide several days of anti-oxidative activity. Additionally, *in vitro* studies with BV-2 microglia cells indicated a significant reduction of intracellular and extracellular reactive oxygen species when cultured on composite MnTBAP surfaces.

1. Introduction

Intracortical microelectrodes are implanted into the cerebral cortex to record changes in neural activity which can be directly related to a variety of essential behavioural and motor-based states[1]. Microelectrode-mediated recordings in animals have advanced our fundamental understanding of brain function in both normal and diseased states[2-4]. In paralyzed individuals, chronic microelectrode recordings promise a way to provide control of various assistive devices[5,6]. Unfortunately, the implementation of intracortical microelectrodes for brain computer interface applications has been severely hindered by inconsistent recording and premature microelectrode failure[7].

The ability of intracortical microelectrodes to record 'usable' activity from single neurons is directly related to the proximity of viable neurons to functional recording sites[8]. Therefore, the most widely accepted theories regarding microelectrode failure focus on changes in the viability and function of neurons near the microelectrode recording sites[9] and damage to the electrode itself, including both the recording sites as well as insulating and passivating coatings[10, 11]. Changes in both viable neuron populations and degradation of the microelectrode itself can be largely attributed to the neuroinflammatory response to the implanted microelectrodes[12].

Consequently, efforts have been made to minimize the reactive tissue response to intracortical microelectrodes. The most promising strategies have targeted inhibition of microglia and macrophage activation, or stabilization of the blood-brain barrier through various materials-based[13-16] and therapeutic strategies[17-19]. Of note, we recently identified a key role for oxidative stress-mediated events following microelectrode implantation in the cerebral cortex[16, 17, 20, 21]. We have found that short-term systemic or localized delivery (up to 48 hours release) of natural anti-oxidants, resveratrol or curcumin, can significantly improve neuronal viability and attenuate neuroinflammation encompassing implanted intracortical microelectrodes[16, 17]. However, short-term anti-oxidant administration was unable to provide sustained neuroprotection (> 4 weeks) around implanted devices. We hypothesized that

the lack of sustained neuroprotection was based on fast clearance rates and low bioavailability[22-24].

In an attempt to combat the limitations of systemic and/or local anti-oxidant delivery, multiple groups have demonstrated the success of immobilized anti-oxidative approaches in mitigating inflammatory pathways following device implantation[25, 26]. For example, Cheung *et. al*. demonstrated that immobilization of a custom superoxide dismutase (SOD) mimetic into a hydrogel system could reduce the formation of reactive oxygen species and improve cell viability[25, 27].

Therefore, the goal of this study was to develop a sustained anti-oxidative coating for intracortical microelectrode applications, based on the immobilization of mimetic SOD. Here, we focused on the characterization and *in vitro* evaluation of a composite coating of the SOD mimetic Mn(III)tetrakis(4-benzoic acid)porphyrin (MnTBAP). Our coating was designed to provide a synergistic initial and sustained anti-oxidative effect. The system was designed to account for future *in vivo* studies, where an initial release is provided to minimize neuron loss following device implantation, while a covalently immobilized layer of MnTBAP is designed to regulate chronic neuroinflammation.

2. Experimental Methods

2.1 Chemicals and Reagents

Mn(III)tetrakis(4-benzoic acid)porphyrin (MnTBAP) was purchased directly from EMB Millipore (Billerica, MA). Glass coverslips (12 mm, No. 1.5), ethanol (EtOH) and hydrochloric acid (HCl) were purchased from Fisher Scientific. All other utilized reagents and solutions were purchased from Sigma Aldrich.

2.2 MnTBAP Substrate Modification

Immobilization of MnTBAP onto silicon dioxide (glass coverslips) was performed using established protocols for biomolecule immobilization[28], with slight modifications. For proof of concept, glass coverslips were used as our substrate to easily translate our methods to coat silicon or polymer based microelectrodes for in vivo studies. A summary of the total reaction scheme used here has been shown in **Figure 1**.

First, glass coverslips were cleaned by submersion in hot (70° C) 2M HCl under constant agitation with a stir bar for 1 hour. Care was taken to ensure that glass coverslips were not shattered during agitation. Following acid treatment, coverslips were washed using an EtOH gradient (95%-70%-50%) and then thoroughly rinsed with deionized water. Following cleaning, coverslips were dried under a stream of nitrogen and placed in a Nordson MARCH PX-250 Plasma Cleaning System (Concord, CA) powered by an MKS ACG-3B RF Plasma Generator (Andover, MA). The coverslips were then exposed to oxygen plasma under vacuum (900 mTorr O2, 25 W, 25 sec.), in order to remove any remaining contaminants and fully oxidize the glass surface. Plasma oxidation of substrates can be performed on nearly any substrate utilized in microelectrode designs, thus demonstrating the broad applicability of our approach. Following plasma treatment, the coverslips were stored in deionized water until use to preserve the cleaned and oxidized surfaces. Plasma treated surfaces were used a maximum of 10 days after initial treatment.

Next, oxidized glass coverslips were placed into a 2% solution of (3-aminopropyl)triethoxysilane (APTES) diluted in toluene (100° C for 1 hour). The glass coverslips were then thoroughly washed, under sonication, two times each, with toluene, 95%

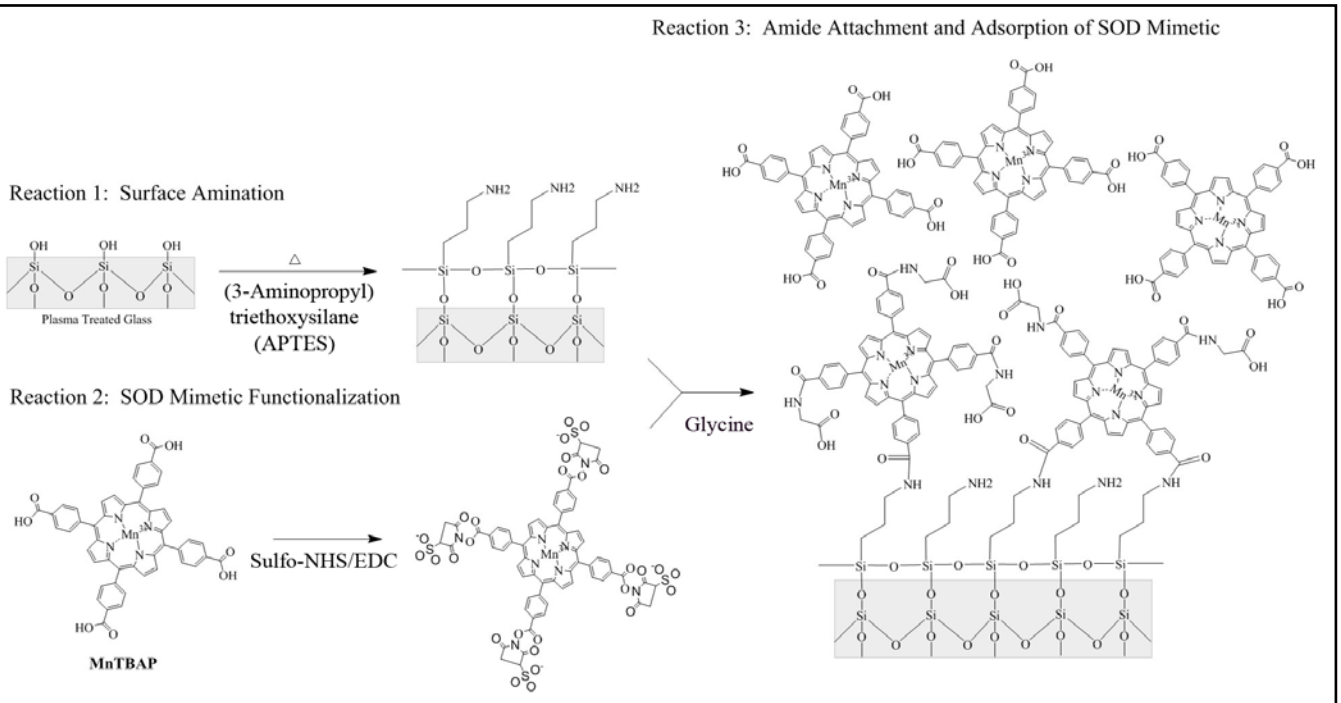

Figure 1. Reaction scheme for synthesis of MnTBAP modified glass surfaces.

ethanol and deionized water for five minutes each. Following washing, coverslips were dried under a stream of nitrogen and cured (110° C for 15 minutes), and stored at 37° C in deionized water for up to 2 days, until use.

In parallel, commercially available MnTBAP (see Section 2.1) was prepared for covalent immobilization to modified glass coverslips. To functionalize MnTBAP, 3 mL of a 4.7 mM aqueous solution of MnTBAP was diluted to 2.4 mM in 4 mM EDC (1-ethyl-3-(3-dimethyl-aminopropyl) carbondiimide hydrochloride), 10 mM NHS (N-hydroxysuccinimide) in 0.1 M 2-(N-morpholino)-ethanesulfonic acid and 0.5 M NaCl, pH 6.0. After 30 minutes at room temperature, the reaction was quenched with 2-mercaptoethanol (20 mM for 5 minutes).

Finally, APTES modified substrates were incubated in functionalized MnTBAP (22 to 24 hours at room temperature). Following incubation, coverslips were thoroughly washed three times with deionized water, 95% EtOH, and then deionized water. For assessment of covalent attachment, a subset of MnTBAP functionalized surfaces were washed three times with deionized water under sonication. After washing, unreacted succinimidyl esters were quenched in 20 mM glycine for 10 minutes. MnTBAP conjugated coverslips were then thoroughly washed in deionized water and stored at 37° C in deionized water until use.

For the purpose of this work, Day 0 was defined as the time point immediately following the final washing.

2.3 Surface Characterization

2.3.1 Contact Angle Measurement: *Determination of Surface Hydrophobicity of Substrates*

Surface hydrophobicity was measured to track the progression of surface modification reactions. Briefly, the contact angle of glass coverslips at each major stage of the coating process was measured using the sessile drop method on a custom-built goniometer (deionized water, 8 µl drop size). In the case of APTES and MnTBAP coated coverslips, measurements were done within 5 days of modification. All surfaces were thoroughly dried under a stream of nitrogen before measurement. Images of the water droplets were taken with a Tucsen TCA 1.31C camera and the droplet angles were later measured using a custom Matlab program. Three separate batches of each surface were fabricated for analysis (N=3, n=9). The contact angle was measured on three material samples from each batch and averaged.

2.3.2 X-ray Photoelectron Spectroscopy (XPS): *Determination of Atomic Composition of Substrates*

Coated glass surfaces were analyzed for elemental composition using a PHI VersaProbe XPS Microprobe (Chanhassen, MN) at the Swagelok Center for Surface Analysis of Materials, Case Western Reserve University. Each sample was scanned using a 15° incident angle, averaging the signal over a 0.1x1.4 mm area (100 µm ion beam size). Survey scans were performed over 0 - 1,100 eV with a pass energy of 93.90 eV.

2.3.3 Quartz Crystal Microbalance: *Determination of MnTBAP Surface Density*

Surface density of conjugated and unconjugated MnTBAP was determined using a quartz crystal microbalance with dissipation (QCMB-D; Qsense E1). SiO_2 sensors were first cleaned using a 30 minute wash in 2% sodium dodecyl sulphate. Sensors were then thoroughly washed in water, dried under nitrogen, plasma treated and APTES coated as outlined above.

APTES coated sensors were then placed in the flow module and a baseline measurement was established by flowing deionized water over the sensor at a rate of 150 µL per minute. All frequency and dissipation measurements were recorded and monitored using the QSOFT software system (Qsense). After a baseline was found, functionalized MnTBAP was flowed over the sensor at the same rate until a plateau was found (~500 µL). Upon plateau, the fluid pump was turned off and the MnTBAP was allowed to interact with the surface of the sensor for 22 to 24 hours. Sensors were then washed as described above, until a baseline frequency and dissipation curve was established. Similar to glass coverslips, the sensor surface was then exposed to 20 mM glycine, and washed with water. The frequency and dissipation baseline following the final water wash was used for quantification.

Data was modelled using the QTOOLS software. Since our system demonstrated viscoelastic properties, surface densities of conjugated MnTBAP were calculated using a Voigt model[29]. A minimum of three harmonics (overtones 3, 5 and 7) was required for computational modelling. Four separate sensors were tested for analysis (n=4).

2.4 Activity of MnTBAP-modified Surfaces

On day 0, 1, and 2 following surface modification, superoxide dismutase activity of MnTBAP-modified surfaces was confirmed using a nitroblue tetrazolium (NBT)/riboflavin (RF) assay[30]. Within the NBT/RF method, RF generates superoxide anion under illumination which reduces NBT, producing a blue dye[30]. In our system, conjugated MnTBAP competes with NBT, directly inhibiting the formation of reduced NBT[31]. Therefore we monitored the inhibition of NBT reduction.

The NBT/RF assay in this work followed previously outlined methods, with minor alterations[32]. Briefly, surfaces were placed into 1.5 mL of a reaction mixture containing phosphate buffer, (50 mM KH_2PO_4, 0.1 mM EDTA, pH 7.8) 2 mM riboflavin, and 57 µM NBT. Samples were incubated in the dark at 4° C for 30 minutes. Following incubation, samples were subsequently illuminated for 15 minutes by two fluorescence tubes (Sylvania, 32 watts) in a foil lined container. Following incubation, the reaction was stopped using a 1:1 addition of chloroform under vortexing. Finally, 100 µL of the organic layer from each sample was measured for absorbance at

560 nm on a SpectraMax M2e spectrophotometer. The percent activity of MnTBAP-modified surfaces was calculated using **Equation 1**:

$$\% \, NBT \, Activity = \frac{\frac{(A-B)}{A}}{C} * 100 \qquad (1)$$

Here, A is the absorbance of solutions incubated with plasma treated glass, B is the absorbance of solutions incubated with the MnTBAP coated surface and C was the absorbance of the amount of soluble MnTBAP on composite surfaces (see Section 2.5). Assays were run a minimum of three times in triplicate (N = 3, n=9).

2.5 Activity of MnTBAP in Solution

To distinguish the impact of the soluble vs immobilized MnTBAP, additional tests were conducted to determine the activity of soluble MnTBAP in solution. Here, the amount of mimetic, as determined using the surface densities of MnTBAP measured using QCMB, was assessed under a NBT/RF assay. Specifically, since our coverslips had an area of 1.13 cm^2, and the determined surface density using QCMB was 21.9 $\mu g/cm^2$, our soluble stock solution was made by combining 24.75 μg of MnTBAP into 100 μL of 50% ethanol.

The NBT assay was run using the same procedure as modified surfaces (See Section 2.5.4) with one modification. Here, 100 μl of soluble MnTBAP solution (0.2475 μg/μL) was added to reach the final volume of 1.5 mL reaction buffer. Following the assay, a chloroform extraction was performed as outlined above to ensure MnTBAP absorbance would not confound the measured NBT absorbance. The chloroform extract was read and 560 nm, and the absorbance was reported according to **Equation 1**. Where here, A was the absorbance of ethanol only and B was the absorbance of the MnTBAP containing solution.

2.6 Intracortical Microelectrode Implantation and Resveratrol Measurement

To better understand the utility of our surfaces, we compared the anti-oxidative activity of MnTBAP-modified surfaces with the anti-oxidative activity of detected levels of resveratrol, a known anti-oxidant, measured around an implanted microelectrode following systemic resveratrol administration. All procedures complied with the Case Western Reserve University Institutional Animal Care and Use Committee (IACUC).

Surgical procedures followed our previously reported methods[17]. Here, immediately following device implantation, a subset of animals received an intraperioteneal injection of 30 mg/kg resveratrol, as previously described[17]. At both 1 and 18 hours after surgical implantation, animals were heavily anesthetized using a mixture of ketamine (80 mg/kg) and xylazine (10 mg/kg) and underwent a cardiac perfusion with 1X PBS. The brain tissue was carefully extracted and a 3-mm biopsy punch was used to extract cortical tissue around the implanted intracortical microelectrode. For this extraction, the electrode site was placed in the middle of the punch allowing for an approximate 1.5 mm radius of tissue to be extracted around the implanted device. All samples were placed in 50% ethanol to extract the resveratrol into the organic phase.

Tissue samples were then thoroughly homogenized and centrifuged to remove tissue and cell debris. The supernatant was measured in a fluorescent plate reader (excitation: 315 nm, emission: 385 nm) to determine the amount of resveratrol that accumulates in the cortical tissue adjacent to the implanted microelectrode. Absolute values were established for resveratrol using a standard curve generated from stock ethanolic solutions. Data are reported as a concentration based on the extracted tissue volume.

Based on the found concentration range of resveratrol found around implanted electrodes, and as a control, the NBT activity of 5 to 25 μM resveratrol was also tested. NBT activity was determined following methodology to soluble MnTBAP (See Section 2.5). For all assays, a stock solution of 100 μM resveratrol in 50% ethanol was serially diluted until the tested concentration range was obtained. Where, for our outlined assay, concentrations below 5 μM could not be tested due to sensitivity limitations.

2.7 *In vitro* Assessment

Glass coverslips and MnTBAP composite coverslips were used for *in vitro* assessment. Before exposure to cells, coverslips were sterilized under ultraviolet light for 15-30 minutes. An immortalized murine microglial cell line (BV-2) was generously donated from Dr. Stephen Selkirk, L. Stokes Cleveland Department of Veterans Affairs, for *in vitro* experiments. BV-2 cells were maintained in DMEM Dulbecco's Modified Eagle Medium (ATCC) supplemented with 10% fetal bovine serum (Invitrogen) and 1% penicillin-streptomycin (ATCC). For all experiments, BV-2 cells were used between passages 5 to 15. For all *in vitro* tests, BV2s were seeded at a density of 250 cells/mm^2 directly on each coverslip.

2.7.1 Intracellular superoxide anion accumulation

Dihydroethidium (DHE) labelling was utilized to measure intracellular superoxide anion accumulation[33]. BV-2 cells were cultured on silicon substrates for 48 hours, washed three times with 1X PBS, and then incubated 3 μM DHE in PBS (30 minutes at room temperature). After three subsequent washes in 1X PBS, samples were transferred to a black well plate and read for total fluorescence (excitation 480 nm, emission 586 nm). Data were reported as a total fluorescent intensity and was conducted a minimum of three times in triplicate (N = 3, n=9).

2.7.2 Soluble nitric oxide and superoxide anion

The levels of soluble nitric oxide were measured from the media of BV-2 cells cultured on sample surfaces for 48 hours using a Greiss Reagent Kit (Life Technologies). Briefly, equal parts of N-(1-naphthyl)ethylenediamine and sulfanilic acid were mixed together to form the Griess reagent. Greiss reagent was added to our samples and incubated for 30 minutes at room temperature. The absorbance of the samples was measured using a microplate reader at 548 nm. Using a standard curve of nitrite concentrations, data was reported as total nitrite concentration.

Additionally, superoxide dismutase activity was measured for samples incubated with cells for 48 hours. Here, culture media was collected for analysis following methods described above in Section 2.4, with slight modification. Specifically, addition of riboflavin was not performed, as the amount of reduced NBT from the media was used to indicate the amount of ROS. In addition, a chloroform extraction was not performed since extraction methods precipitated serum proteins in the media, complicating signal analysis.

2.7.3 Live/Dead Assay

Cell viability was assessed to ensure the surface modifications were not inducing adverse cytotoxic effects. The LIVE/DEAD® Viability/Cytotoxicity Kit (Life Technologies) was utilized with slight modifications. Here, glass and MnTBAP treated coverslips were tested. Positive (all live) and negative (all dead) controls were performed utilizing clean glass coverslips. The negative control was established by incubating cells with 70% methanol for 10 minutes. Cells were seeded for 48 hours prior to removal of media and incubated in 8 uM ethidium homodimer-1 (EthD-1) and 0.1 uM calcein-AM in complete PBS for 15 min. The samples were then washed once with 1xPBS. For quantification, cell-seeded samples were transferred to a black well plate for a total fluorescence read on the plate reader of EthD-1 activity (excitation 528 nm, emission 617 nm). Percentage of dead cells was calculated by normalizing total fluorescent intensity to the negative controls (N=3, n=9).

Representative images from live/dead and DHE assays were acquired fluorescently using an inverted AxioObserver Z1 (Zeiss) equipped with an AxioCam MRm prior to detection on the plate reader, to confirm measured values. For each assay, exposure times were held constant between conditions.

2.8 Statistical Analysis

For all conducted experiments, a minimum of three trials (N=3, n=9) were used for statistical evaluation (N≥3). For the Live/Dead assays a one-way analysis of variance (ANOVA) with a Tukey's post-hoc test was used to find significance. For all other assays, a standard student t-test was utilized to determine significance. In all cases statistical significance was defined as $p<0.05$.

3. Results and Discussion

3.1 Design of Synthetic Anti-oxidative Modified Substrates

Building on our previous work with the anti-oxidant resveratrol, we sought to engineer a surface modification that would provide an initial release of anti-oxidative activity to mimic results found in our previous work. In addition, our goal was to also ensure that our engineered substrates would improve the longevity of local anti-oxidative effects. Therefore, we designed an anti-oxidative surface treatment that provided an initial release of anti-oxidant, followed by sustained anti-oxidative activity. To achieve our desired surface modifications, we focused on the characterization and *in vitro* evaluation of a composite coating of the SOD mimetic Mn(III)tetrakis(4-benzoic acid) porphyrin (MnTBAP) (**Figure 1**).

A key advantage of MnTBAP and other metalloporphyrins are their ability to repeatedly scavenge reactive oxygen species[34, 35]. The two half reactions enabling MnTBAP to repeatedly scavenge superoxide anion are shown in **Equation 2**.

$$Mn^{2+} + O_2^- + 2H^+ \rightarrow Mn^{3+} + H_2O_2 \quad \textbf{(2i)}$$

$$Mn^{3+} + O_2^- \rightarrow Mn^{2+} + O_2 \quad \textbf{(2ii)}$$

A number of studies have shown MnTBAP to be stable in aqueous media for extended periods[36-38]. Due to the small size and chemical structure, MnTBAP is also capable of crossing biological membranes, enabling MnTBAP to act within the cell, as well as extracellularly[39-41].

The ability of MnTBAP to stably and repeatedly scavenge reactive oxygen species (ROS) is of critical importance for the application of intracortical microelectrodes. Specifically, multiple groups have suggested a key role of ROS in mediating corrosion of electrical contacts ultimately resulting in microelectrode failure[10, 11, 42]. In fact, a recent study by Barrese *et al* suggested that the majority of chronic Utah electrode array failures could be attributed to corrosion and/or degradation of electrode insulation[10]. Further, it has also been suggested that the high biocompatibility of platinum microelectrodes in the brain, versus other metals such as tungsten, may be due to platinum's ability to directly act as an anti-oxidant[42]. In addition, we have shown a correlation between neuronal health and intracellular accumulation of ROS around implanted microelectrodes[17]. Therefore, given the versatility of MnTBAP, and the impact of ROS on intracortical microelectrode stability, our approach promises to become an excellent candidate for *in vivo* applications of intracortical microelectrodes.

Composite coatings of the MnTBAP SOD mimetic were created by first functionalizing plasma treated glass (SiO_2) coverslips with (3-aminopropyl)triethoxysilane. In order to confirm amine functionalization of the plasma treated silicon substrates, both the hydrophobicity and atomic composition were characterized with goniometry (**Table 1**) and XPS (**Table 2**), respectively. Consistent with literature values[43], surface

amination caused an increase in contact angle from < 5° ± 0 to 55.2° ± 2.8°. Additionally, XPS analysis confirmed grafting to the anime terminated silane. Specifically, XPS analysis demonstrated a reduction in the composition of both oxygen (68.8% to 39.0%, **Table 2**) and silicon (27.3% to 16.9%), and an increase in both carbon (3.8% to 38.1%) and nitrogen (<0.1% to 6.0%), consistent with published values[44]. The amine modified substrate was designed for both covalent immobilization of the MnTBAP through succinimidyl ester coupling[28, 45], and to facilitate more natural conformations of non-specifically adsorbed protein in future *in vivo* studies (**Figure 1**)[46].

Table 1. Contact Angle Measurements on Modified Surfaces.

Surface	Contact Angle
Plasma treated SiO_2	< 5° ± 0 [a]
Amine functionalized	55.2° ± 2.8°
MnTBAP SOD mimetic composites	24.3° ± 1.4°

[a]Surface wetting was < 5°, which was below the detectable region

Sulfo NHS-ester functionalized MnTBAP SOD mimetics were subsequently exposed to the anime functionalized substrates to create a composite coating. The composite consisted of both covalent immobilized and non-specifically adsorbed MnTBAP (**Figure 1**). Both contact angle measurements and XPS analysis confirmed the surface coating of MnTBAP SOD mimetics. Goniometry indicated a reduction in contact angle from 55.2° ± 2.8° to 24.3° ± 1.4° (**Table 1**). Additionally, XPS analysis confirmed a reduction in the composition of nitrogen (6.0% to 3.1%, **Table 2**), and an increase in both carbon (38.1% to 47.1%) and Mn (<0.1% to 0.5%). Passively adsorbed MnTBAP could be mechanically removed with cotton swabs, or additional washing with EtOH. Removal of the adsorbed MnTBAP and subsequent analysis with XPS indicated no significant difference in the atomic composition of the substrates, compared to MnTBAP SOD mimetic composites

Table 2. XPS Analysis on Modified Surfaces

Modification	O (%)	Si (%)	C (%)	N (%)	Mn (%)
Plasma treated SiO_2	68.8	27.3	3.8	<0.1	<0.1
Amine functionalized	39.0	16.9	38.1	6.0	<0.1
MnTBAP SOD mimetic composites	36.3	13.1	47.1	3.1	0.5
MnTBAP SOD mimetic covalent immobilized only	34.2	13.2	47.9	4.2	0.5

In order to determine the surface density of our composite MnTBAP substrates, we utilized a quartz crystal microbalance (QCMB). QCMB allowed for the real-time evaluation of the evolution of the MnTBAP SOD composite. Using a Voigt model, the change in frequency after the finalized chemical reaction indicated a mass increase of 21.9 μg/cm^2, for the MnTBAP composite surfaces. However, the chemical compatibility limits of our QCMB did not allow for additional steps that would have given us a definitive evaluation of surfaces with only covalently attached MnTBAP.

3.2 Anti-oxidative Activity of MnTBAP-modified Surfaces

In order to determine the anti-oxidative activity of the SOD mimetic modified surfaces, we utilized the Riboflavin/NitroBlue Tetrazolium (RF/NBT) assay. Under illumination, RF generates a superoxide O_2^- radical that will reduce the NBT. In the presence of an antioxidant, the reduction of NBT is inhibited. In this assay, SOD mimetics (or resveratrol in the case of control experiments) compete with NBT for the superoxide O_2^- radical. Therefore, **Figure 2** presents the anti-oxidative activity of each surface treatment as the % Inhibition of NBT Reduction by RF, normalized to the activity of plasma treated silicon substrates. As a control, the amount of soluble MnTBAP on the composite surfaces was run prior to surface testing. Specifically, given the QCMB determined surface density and area of coverslip, the anti-oxidative activity of 24.75 μg of soluble MnTBAP was utilized as a reference and noted as 100%. Therefore, 100% inhibition of NBT reduction was defined as the reduction demonstrated by soluble MnTBAP equivalent to the amount immobilized on the composite surface (**See Equation 1**).

As an additional control, we compared the activity of our

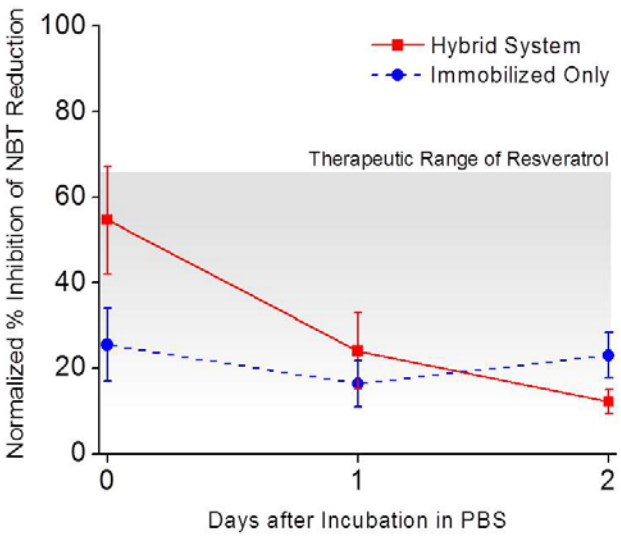

Figure 2. Activity of MnTBAP composite surfaces over time. The ability of anti-oxidative surfaces to prevent NBT reduction was measured up to two days after synthesis and incubation in PBS. Hybrid (composite) surfaces (red square) demonstrated an initial decline in NBT reduction activity, followed by low-level sustained activity. In contrast, surfaces with only conjugated MnTBAP maintained activity over time (blue circle). Data was normalized to soluble MnTBAP (0.24 μM). Grey region represents the working therapeutic range for resveratrol. Data is shown as an average ± s.e.m. N=3, n=9.

modified surfaces to the natural anti-oxidant resveratrol. We have previously demonstrated that administration of resveratrol the day before and the day of microelectrode implantation provides neuroprotection at the implant site for up to four weeks[17]. Therefore to ensure that our surfaces had similar anti-oxidative properties to our previous study, here we report on: (1) the concentration of accumulated resveratrol around the cortical tissue adjacent the microelectrode up to 48 hours after electrode implantation and (2) the relative NBT activity of the measured resveratrol concentration in comparison to soluble MnTBAP and our modified surfaces.

Resveratrol is a conjugated bi-phenol, and naturally fluoresces at 385 nm. Therefore, following our two-dose administration of resveratrol, cortical tissue adjacent to the microelectrode was retrieved from euthanized animals. Resveratrol was extracted from tissue as described above, and the concentration of resveratrol within the tissue was determined spectophotometrically against a standard curve. We found that our dosing scheme resulted in a concentration range of resveratrol of between ~0.5 to 25 μM for up to 48 hours after injection/implantation (**Figure 3**). Interestingly, several groups, including ours, have also shown high efficacy and low toxicity of resveratrol from 5 to 25 μM *in vitro*[20, 47].

Most importantly, we found that within this concentration range, resveratrol provided significant levels of anti-oxidative activity. Specifically, a concentration of 25 μM of resveratrol had the ability to inhibit approximately 65 ± 9.7% of NBT reduction capabilities of soluble MnTBAP.

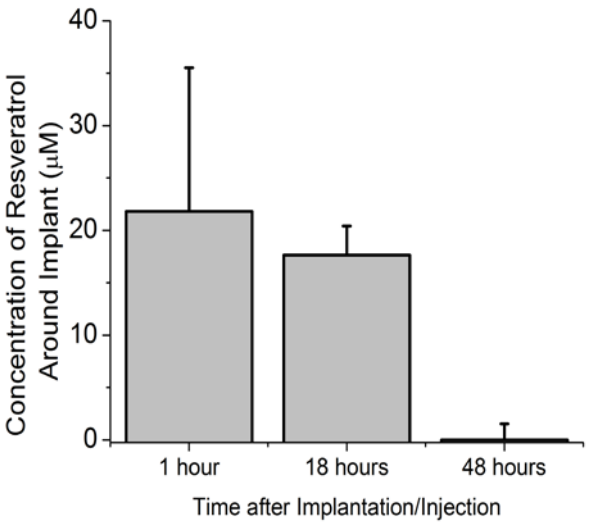

Figure 3. Bio-distribution of resveratrol around implanted microelectrodes up to 48 hours after administration. A therapeutic range (5 to 25 μM) was found around implanted devices for up to 18 hours after implantation. Concentration is reported as an average ± s.e.m. (n≥3).

After immobilization, MnTBAP composite surfaces maintained nearly 60% of the activity of the soluble MnTBAP (**Figure 2**). Further, at early time points, MnTBAP composite surfaces were capable of similar anti-oxidative activity to the levels facilitated by the upper limits of resveratrol detected at the microelectrode surface 1-18 hours after administration (**Figure 3**). Specifically, we found that the NBT inhibition ability of our composite MnTBAP surfaces was statistically similar to the peak tested concentration of resveratrol (25 μM) at day 0. Despite a decline in activity after day 0, at both days 1 and 2, the anti-oxidative activity of MnTBAP composite surfaces was statistically similar to the lower end of functional resveratrol concentrations (**Figure 2**, 5 μM). Although our MnTBAP composite surfaces displayed a sustained anti-oxidative property, further testing would be required to determine the effect of prolonged activity on neuroprotection.

In order to confirm the source of the decline in anti-oxidative activity of composite surfaces, immobilized only surfaces were created. At time 0, approximately 45% of the anti-oxidative activity demonstrated from the composite surfaces was generated from the surface immobilized MnTBAP. Upon testing at subsequent time points, we found no statistical differences between the immobilized only and composite surfaces (**Figure 2**). In comparison to the hybrid composite surfaces, it would appear that the adsorbed layer of MnTBAP disassociates from the surface within 24 hours from exposure to physiologically relevant systems. Most importantly, the activity of the immobilized MnTBAP remained consistent during the extent of our initial testing, and provided statistically similar anti-oxidative activity to therapeutically relevant levels of resveratrol (5 μM[20], **Figure 2**). Further, our results also demonstrate, for the first time to our knowledge, that covalent immobilization of MnTBAP is capable of physiologically relevant anti-oxidative activity (**Figure 2**).

It is important to note that without the adsorbed layer of MnTBAP, our composite surfaces would not be fully capable of similar high anti-oxidative activity provided by resveratrol early after administration. Specifically, for all investigated time points, surfaces with only immobilized MnTBAP had significantly less NBT reduction activity than 25 μM of resveratrol. However, hybrid systems had similar activity to resveratrol at Day 0 post synthesis. Further, maintained activity was noted in hybrid surfaces, and by day 1 and 2, no significant differences from 5 μM of resveratrol were noted. Thus, the hybrid composite MnTBAP surface provides distinct advantages to both soluble resveratrol delivery and surface immobilization only of MnTBAP, without the deliverable adsorbed layer.

3.3 Effect of MnTBAP-modified Surfaces on Reactive Oxygen Species and Nitric Oxide Accumulation and Release

Following validation of active MnTBAP composite surfaces, we utilized *in vitro* evaluation to determine the effects of our engineered systems on activated microglia cells. Specifically, for our analysis we utilized an immortalized murine microglia cell line that we have found is constitutively in the M1 pro-inflammatory phenotype as shown by $CD86^+$ and $CCR7^+$ labelling (data not shown). Other groups have suggested the key role of microglia and macrophages in the neuroinflammatory response that exists around intracortical microelectrodes[48-50]. It has been suggested that the formation of neurotoxic regions around the implant is likely the result of an accumulation of M1 phenotypic microglia/macrophage population[51,52]. Further, given that M1 microglia and macrophages primarily release high amounts of ROS[53], it is also probable that microglia and macrophage cells are involved in the corrosion of the actual microelectrode. Therefore, we investigated the ability of the anti-oxidative MnTBAP composite surfaces to prevent ROS accumulation and release from activated M1 phenotypic microglia cells seeded on our modified materials.

First we investigated the accumulation of ROS in microglia cells. Specifically, to label intracellular accumulation of ROS, we utilized dihydroethidium (DHE), a dye that selectively immobilizes inside the cell upon reaction with superoxide anion. Thus, increased DHE positive labelling would infer more intracellular superoxide anion within the cells. Here we found that microglia cells seeded on MnTBAP composite surfaces demonstrated significant decreases in intracellular superoxide anion compared to unmodified glass substrates (**Figure 4**).

Changes in intracellular ROS accumulation can directly affect the anti-oxidative properties within an inflammatory cell[54, 55]. Further, increases in intracellular ROS can also result in the accelerated release of ROS into the local extracellular environment[56, 57]. In the case of intracortical microelectrodes, increases in extracellular ROS in the local environment could result in both (1) neuronal cell death[17] and/or (2) corrosion of the insulating and conducting layers on the electrode[10, 42, 58]. Therefore, it is also critical that we evaluated the effects of our MnTBAP hybrid surfaces on extracellular ROS released from activated M1 microglia cells.

The effect of MnTBAP modified surfaces on the accumulation of cell-released ROS was investigated using a modified NBT assay. Specifically, neat NBT was added to tissue culture medium and the amount of NBT dye reduction was quantified. The amount of ROS in solution is therefore directly proportional to the amount of NBT dye reduction; a surface modification that demonstrated more NBT reduction would indicate higher levels of ROS accumulation. Notably we found that our MnTBAP composite surfaces were capable of

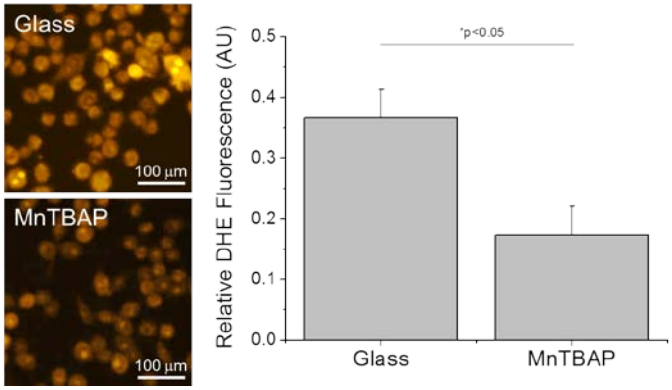

Figure 4. Accumulation of intracellular superoxide anion (dihydroethidium; DHE) from activated microglia cells (BV2s) 48 hours after seeding onto modified surfaces. Cells seeded on MnTBAP modified surfaces demonstrated a significant reduction (*p<0.05) in DHE labelling. N=3, n=9.

significant decreases in soluble ROS accumulation from activated M1 microglia cells (**Figure 5**).

We have previously shown that reduction of ROS around implanted microelectrodes directly correlates with a more stable blood-brain barrier and more viable neurons[17]. Thus, we wanted to ensure that the mimetic employed here would be capable of similar protection. Based on this input criteria, MnTBAP, was chosen due to its ability to selectively alter the release and accumulation of reactive oxygen species (ROS) in contrast to nitric oxide. The selectivity of MnTBAP was critical given the role of nitric oxide in cortical tissue. Specifically, in homeostasis, nitric oxide, being freely able to pass the blood-brain barrier, has been identified as a key messenger molecule in brain tissue[59]. The synthesis and release

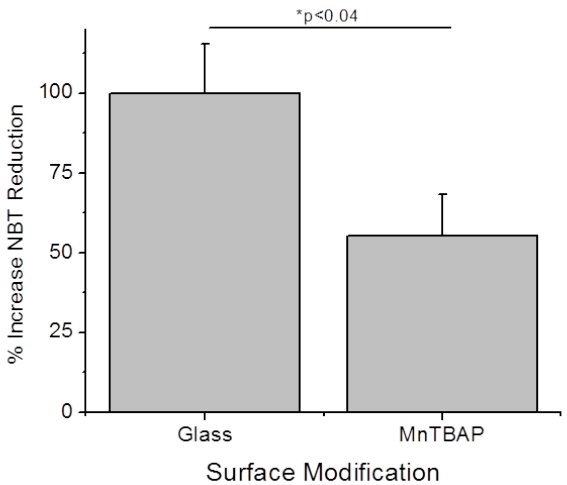

Figure 5. Release of reactive oxygen species (ROS) from activated microglia cells (BV2s) 48 hours after seeding onto surfaces. Cells seeded onto MnTBAP modified surfaces released a significantly smaller amount of ROS in comparison to glass controls (*p<0.04). N=3, n=9.

of nitric oxide has been correlated with neuronal activity, cerebral blood flow and glial cell homeostatic function[60, 61]. In contrast, during inflammatory states, nitric oxide can be pro- and anti-inflammatory[62]. Particularly, only in the presence of ROS can nitric oxide be reacted to form reactive peroxynitrite ($ONOO^-$)[59, 63], a molecule known to be in high amounts during oxidative stress and inflammatory states. In our model, we aimed to specifically reduce ROS to prevent direct neurotoxicity and to prevent the accumulation of nitrite anion.

Therefore, to confirm the specificity of MnTBAP in our model, we tested the effect of our MnTBAP composites on nitric oxide (NO) release and accumulation from cultured activated microglia. After two days of incubation on our surfaces, we found that MnTBAP modifications did not result in any significant changes in NO release from microglia cells in comparison to glass controls, as expected (data not shown). In addition, it has been previously demonstrated that only concentrations above 25 μM of resveratrol have been shown to substantially alter nitric oxide concentrations[64].

3.4 Effect of MnTBAP modified surfaces on cellular viability

Taken collectively, our results suggested that our MnTBAP SOD mimetic composite surfaces were capable of reducing both intracellular and extracellular reactive oxygen species. However, to ensure that the molecular changes that were noted in activated microglia cells were not the result of changes in cell viability, we conducted a Live/Dead cell cytotoxicity assay on seeded microglia cells. Notably, we found that MnTBAP modified surfaces had statistically similar levels of live and dead cells in comparison to glass controls (**Figure 6**). Therefore, our results suggested that our reported changes in cellular accumulation and release of ROS from MnTBAP modified surfaces were likely the result of our engineered surfaces, and not the result of changes in cell viability after seeding.

In addition, the results presented in **Figure 6** are desirable given the critical role microglia play in the inflammatory cascade following device implantation[65]. Specifically, microglia cells have been shown to directly adhere to the surface of the electrode[66]. After adhesion, microglia cells begin to release soluble factors that can (1) further activate surrounding cells, (2) affect local neuronal homeostasis and (3) affect the functionality of the actual electrode[52]. Elimination of adherent microglia may result in disruption of the inflammatory response and impede the wound healing process.

Given that we observe reductions in both intra- and extracellular ROS accumulation as a result of immobilized and released MnTBAP, we hypothesize that our hybrid composite surfaces have the ability to interact with microglia cells adherent to the microelectrode, as well as locally activated microglia cells that are responding to the tissue damage and the change in local inflammatory state **Figure 7**. Specifically,

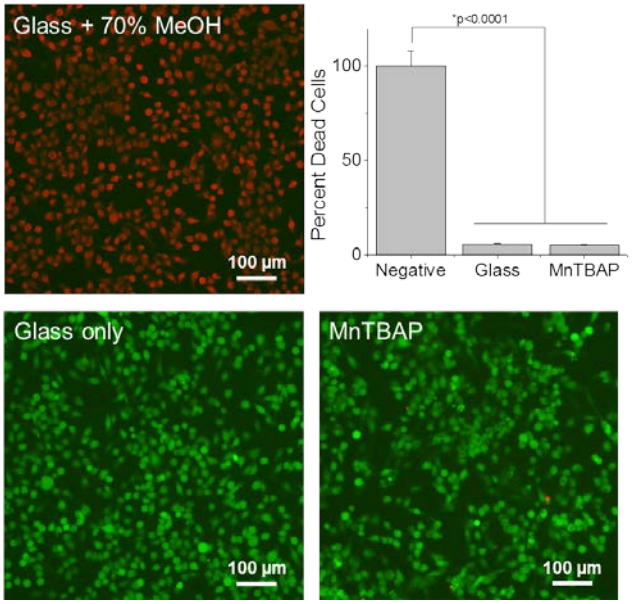

Figure 6. Cytotoxicity of modified surfaces on activated microglia cells (BV2s) after 48 hours. No significant levels of cellular cytotoxicity were noted for investigated modifications. Green denotes live cells and red denotes dead cells. N=3, n=9.

adsorbed MnTBAP, once released, could directly pass through the microglia cell membrane and result in changes in intracellular ROS production and accumulation, similar to those we noted in our study (**Figure 4**). Released MnTBAP could also reduce extracellular ROS accumulation. In addition, covalently immobilized MnTBAP should facilitate the repetitive conversion of extracellular ROS into oxygen in the localized environment (see **Equation 2** and **Figure 5**).

We have previously shown that a stimulant-initiated threshold-dependent response in microglia activation can result in differences in neuronal survival at the microelectrode-tissue interface[21]. Therefore, utilizing redundant mechanisms to decrease of ROS accumulation around the implanted microelectrode increases the probability that our designed surfaces could be a viable option for the prevention of both corrosive damage to the electrodes and inflammatory-mediated neurodegeneration; both leading to improvements to the stability of intracortical microelectrodes following implantation.

4. Conclusions

Neuroinflammation and oxidative stress events have been shown to result in the loss of neuronal bodies around implanted microelectrodes[49, 66]. Therefore, in the present study, we sought to develop anti-oxidative surface modifications to intracortical microelectrodes. Here, we investigated the feasibility of MnTBAP SOD mimetic conjugated surfaces that were capable of an initial release to combat initial neuronal loss and sustained anti-oxidative activity to regulate neuroinflammation. Notably, we found that our engineered systems were capable of anti-oxidative activity up to two days after exposure to

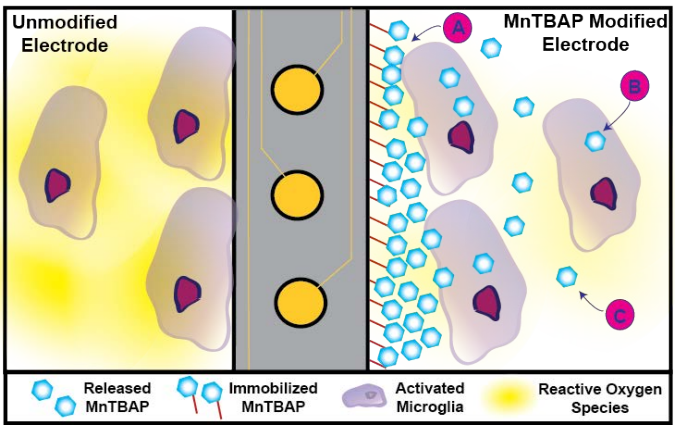

Figure 7. Proposed mechanism of action for MnTBAP composite surfaces. Left: For an unmodified electrode, microglia cells adhere to the surface of the device and release high amounts of reactive oxygen species (ROS). Right: In the presence of our MnTBAP composite surfaces, three possible mechanisms of action could result in decreases in localized ROS released from activated microglia. (A) Immobilized MnTBAP could directly convert extracellular ROS to water. (B) Microglia can internalize released MnTBAP, which could directly decrease the amount of intracellular ROS accumulation. (C) Non-internalized released MnTBAP freely diffuses into the tissue space and can neutralize ROS in the extracellular space.

physiologically relevant conditions. Further, MnTBAP modified surfaces were able to reduce intracellular and extracellular ROS release from activated microglia cells *in vitro*.

It is important to note that the results presented here are of particular interest, since as to date, no group has successfully immobilized a commercially available SOD mimetic to a material surface. Therefore, we anticipate that the modification scheme that has been developed here has the potential to be deployed in several biomedical applications, such as cortical/peripheral neural electrodes, stents, hip implants and cardiac leads. In addition, due to the ability of most materials to be plasma treated, we anticipate our surface modification technique could be employed for many material types including polyimides, parylene-C and polydimethylsiloxane. Finally, given the success of our modified surfaces *in vitro*, future studies will investigate the use of MnTBAP modified surfaces in reducing neuronal cell death and corrosion of intracortical microelectrodes in an *in vivo* model.

Acknowledgements

This work was supported by the Department of Biomedical Engineering and Case School of Engineering at Case Western Reserve University through lab start-up funds, the Department of Education, Graduate Fellowships in neural engineering, GAANN:P200A100112 (K. Potter), and the NIH Neural Engineering and Rehabilitation Training Grant (J. Nguyen), (5T32EB004314-14). Additional funding on this research was supported in part by the Department of Veterans Affairs Merit Review (B7122R), Presidential Early Career Award for Scientist and Engineers (PECASE). The authors have no conflicts of interest related to this work to disclose. None of the funding sources aided in the collection, analysis and interpretation of data, in the writing of the report, or in the decision to submit the paper for publication.

The authors also acknowledge the support of Archana Jaiswal from Biolin Scientific for help in processing quartz crystal microbalance data sets. In addition, the author's also acknowledge the support of S. Selkirk and K. Buchanan.

Notes and references

[a] Department of Biomedical Engineering, Case Western Reserve University, 2071 Martin Luther King Jr Drive, Wickenden Building, Cleveland, OH 44106

[b] Advanced Platform Technology Center, L. Stokes Cleveland VA Medical Center, 10701 East Boulevard Mail Stop 151 AW/APT, Cleveland, OH 44106

Ψ Denotes co-first author.

* Direct correspondence to jeffrey.capadona@case.edu

1. M. Bortole, M. Controzzi, I. Pisotta and A. Úbeda, 2014, **4**, 235-247.
2. D. M. Taylor, S. I. H. Tillery and A. B. Schwartz, *Science*, 2002, **296**, 1829-1832.
3. C. A. Chestek, V. Gilja, P. Nuyujukian, J. D. Foster, J. M. Fan, M. T. Kaufman, M. M. Churchland, Z. Rivera-Alvidrez, J. P. Cunningham, S. I. Ryu and K. V. Shenoy, *J. Neural Eng.*, 2011, **8**, 045005.
4. K. S. Carlson, C. Z. Xia and D. W. Wesson, *J. Neurosci.*, 2013, **33**, 13873-13881.
5. M. A. L. Nicolelis, *Nat. Rev. Neurosci.*, 2003, **4**, 417-422.
6. A. B. Schwartz, *Annu. Rev. Neurosci.*, 2004, **27**, 487-507.
7. J. D. Simeral, S. P. Kim, M. J. Black, J. P. Donoghue and L. R. Hochberg, *J Neural Eng*, 2011, **8**, 025027.
8. G. Buzsaki, *Nat. Neurosci.*, 2004, **7**, 446-451.
9. A. J. Woolley, H. A. Desai and K. J. Otto, *J Neural Eng*, 2013, **10**, 026007.
10. J. C. Barrese, N. Rao, K. Paroo, C. Triebwasser, C. Vargas-Irwin, L. Franquemont and J. P. Donoghue, *J Neural Eng*, 2013, **10**, 066014.
11. A. Prasad, Q.-S. Xue, V. Sankar, T. Nishida, G. Shaw, W. J. Streit and J. C. Sanchez, *J Neural Eng*, 2012, **9**, 056015.
12. S. F. Cogan, *Annual Review of Biomedical Engineering*, 2008, **10**, 275-309.
13. J. Skousen, S. Merriam, O. Srivannavit, G. Perlin, K. Wise and P. Tresco, *Prog. Brain Res.*, 2011, **194C**, 167-180.
14. T. Ware, D. Simon, C. Liu, T. Musa, S. Vasudevan, A. Sloan, E. W. Keefer, R. L. R. II and W. Voit, *Journal of Biomedical Materials Research B*, 2013.
15. J. P. Harris, J. R. Capadona, R. H. Miller, B. C. Healy, K. Shanmuganathan, S. J. Rowan, C. Weder and D. J. Tyler, *J Neural Eng*, 2011, **8**, 066011.
16. K. A. Potter, M. Jorfi, K. T. Householder, E. J. Foster, C. Weder and J. R. Capadona, *Acta Biomaterialia*, 2013, **In Press**.

17. K. A. Potter, A. C. Buck, W. K. Self, M. E. Callanan, S. Sunil and J. R. Capadona, *Biomaterials*, 2013, **34**, 7001-7015.
18. R. L. Rennaker, J. Miller, H. Tang and D. A. Wilson, *J Neural Eng*, 2007, **4**, L1-L5.
19. Y. Zhong and R. Bellamkonda, *J. Controlled Release*, 2005, **106**, 309-318.
20. M. Ravikumar, S. Jain, R. H. Miller, J. R. Capadona and S. M. Selkirk, *J. Neurosci. Methods*, 2012, **211**, 280-288.
21. M. Ravikumar, D. J. Hageman, W. H. Tomaszewski, G. M. Chandra, J. L. Skousen and J. R. Capadona, *Journal of Materials Chemistry B*, 2013.
22. T. Walle, *Ann. N. Y. Acad. Sci.*, 2011, **1215**, 9-15.
23. P. Anand, A. B. Kunnumakkara, R. A. Newman and B. B. Aggarwal, *Molecular Pharmaceutics*, 2007, **4**, 807-818.
24. M. Asensi, I. Medina, A. Ortega, J. Carretero, M. C. Bano, E. Obrador and J. M. Estrela, *Free radical biology & medicine*, 2002, **33**, 387-398.
25. P. S. Hume and K. S. Anseth, *Journal of biomedical materials research. Part A*, 2011, **99**, 29-37.
26. W. He, G. C. McConnell, T. M. Schneider and R. V. Bellamkonda, *Adv. Mater.*, 2007, **19**, 3529-3533.
27. C. Y. Cheung, S. J. McCartney and K. S. Anseth, *Adv. Funct. Mater.*, 2008, **18**, 3119-3126.
28. J. R. Capadona, T. A. Petrie, K. P. Fears, R. A. Latour, D. M. Collard and A. J. García, *Adv. Mater.*, 2005, **17**, 2604-2608.
29. M. V. Voinova, M. Rodahl, M. Jonson and B. Kasemo, *Phys. Scr.*, 1999, **59**, 391.
30. M. V. Berridge, P. M. Herst and A. S. Tan, *Biotechnol. Ann. Rev.*, 2005, **11**, 127-152.
31. I. Batinic-Haberle, S. Cuzzocrea, J. S. Reboucas, G. Ferrer-Sueta, E. Mazzon, R. Di Paola, R. Radi, I. Spasojevic, L. Benov and D. Salvemini, *Free radical biology & medicine*, 2009, **46**, 192-201.
32. P. J. Janknegt, J. W. Rijstenbil, W. H. V. d. Poll, T. S. Gechev and A. G. J. Buma, *J. Photochem. Photobiol. B: Biol.*, 2007, **87**, 218-226.
33. M. Zanetti, L. d'Uscio, T. E. Peterson, Z. S. Katusic and T. O'Brien, in *Methods in Molecular Medicine*, eds. J. P. Fennel and A. H. Baker, pp. 65-72.
34. I. Batinic-Haberle, J. S. Reboucas and I. Spasojevic, *Antioxidants & Redox Signaling*, 2010, **13**, 877-918.
35. C. Li and H.-M. Zhou, *Enzyme Research*, 2011, **2011**, 1-6.
36. M. Zahmatkesh, M. Kadkhodaee, S. M. S. Moosavi, M. Jorjani, A. Kajbafzadeh, A. Golestani and R. Ghaznavi, *Clinical and Experimental Nephrology*, 2005, **9**, 212-218.
37. B. J. DAY, S. SHAWEN, S. I. LIOCHEV and J. D. CRAPO, *Journal of Pharmacology and Experimental Therapeutics*, 1995, **275**, 1227-1232.
38. J. S. L. Mok, K. Paisley and W. Martin, *British Journal of Pharmacology*, 1998, **124**, 111-118.
39. D. Salvemini, C. Muscoli, D. P. Riley and S. Cuzzocrea, *Pulmonary Pharmacology & Therapeutics*, 2002, **15**, 439-447.
40. P. J. F. Gauuan, M. P. Trova, L. Gregor-Boros, S. B. Bocckino, J. D. Crapo and B. J. Day, *Bioorganic & Medicinal Chemistry*, 2002, **10**, 3013-3021.
41. D. Salvemini, D. P. Riley and S. Cuzzocrea, *Nature reviews. Drug discovery*, 2002, **1**, 367-374.
42. E. Patrick, M. E. Orazem, J. C. Sanchez and T. Nishida, *J. Neurosci. Methods*, 2011, **198**, 158-171.
43. L.-S. Jang and H.-J. Liu, *Biomedical Microdevices*, 2008, **11**, 331-338.
44. Y. Han, D. Mayer, A. Offenhäusser and S. Ingebrandt, *Thin Solid Films*, 2006, **510**, 175-180.
45. J. E. Raynor, J. R. Capadona, D. M. Collard, T. A. Petrie and A. s. J. García, *Biointerphases*, 2009, **4**, FA3.
46. B. G. Keselowsky, D. M. Collard and A. J. Garcıa, *Journal of Biomedical Materials Research*, 2003, **66A**, 247-259.
47. B. Turan, E. Tuncay and G. Vassort, *J. Bioenerg. Biomembr.*, 2012.
48. B. K. Leung, R. Biran, C. J. Underwood and P. A. Tresco, *Biomaterials*, 2008, **29**, 3289-3297.
49. V. Polikov, P. Tresco and W. Reichert, *J. Neurosci. Methods*, 2005, **148**, 1-18.
50. D. Szarowski, *Brain Res*, 2003, **983**, 23-35.
51. N. Mokarram, A. Merchant, V. Mukhatyar, G. Patel and R. V. Bellamkonda, *Biomaterials*, 2012, **33**, 8793-8801.
52. N. Mokarram and R. V. Bellamkonda, *IEEE TRANSACTIONS ON BIOMEDICAL ENGINEERING*, 2010, **PP**, 1-1.
53. K. A. Kigerl, J. C. Gensel, D. P. Ankeny, J. K. Alexander, D. J. Donnelly and P. G. Popovich, *J. Neurosci.*, 2009, **29**, 13435-13444.
54. V. Shukla, S. K. Mishra and H. C. Pant, *Adv. Pharm. Sci.*, 2011, **2011**, 572634.
55. A. A. Starkov, *Methods Mol Biol*, 2010, **648**, 245-255.
56. K. Apel and H. Hirt, *Annu Rev Plant Biol*, 2004, **55**, 373-399.
57. B. D'Autreaux and M. B. Toledano, *Nat Rev Mol Cell Biol*, 2007, **8**, 813-824.
58. A. Prasad, Q. S. Xue, V. Sankar, T. Nishida, G. Shaw, W. J. Streit and J. C. Sanchez, *J Neural Eng*, 2012, **9**, 056015.
59. J. Garthwaite and C. L. Boulton, *Annual Reviews in Physiology*, 1995, **57**, 683-706.
60. N. AKGOREN, M. FABRICIUS and M. LAURITZEN, *PNAS*, 1994, **91**, 5903-5907.
61. R. P. Patel, J. McAndrew, H. Sellak, C. R. White, H. Jo, B. A. Freeman and V. M. Darley-Usmar, *Biochim. Biophys. Acta*, 1999, **1411**, 385-400.
62. D. A. Drechsel, A. G. Estevez, L. Barbeito and J. S. Beckman, *Neurotoxicity research*, 2012.
63. T. Mizuno, *Brain Res*, 2003, **979**, 65-70.
64. X. Lu, L. Ma, L. Ruan, Y. Kong, H. Mou, Z. Zhang, Z. Wang, J. Wang and Y. Le, *Journal of Neuroinflammation*, 2010, **7**, 46.
65. P. A. Tresco and B. D. Winslow, *Critical Reviews in Biomedical Engineering*, 2011, **39**, 29-44.
66. R. Biran, D. Martin and P. Tresco, *Exp. Neurol.*, 2005, **195**, 115-126.